



All-in-one strain-triboelectric sensors based on environment-friendly ionic hydrogel for wearable sensing and underwater soft robotic grasping

Juntian Qu^{a,*}, Qiangjing Yuan^a, Zhenkun Li^b, Ziqiang Wang^a, Feng Xu^a, Qigao Fan^c,
Min Zhang^a, Xiang Qian^a, Xueqian Wang^a, Xiaohao Wang^a, Minyi Xu^{d,*}

^a Shenzhen International Graduate School, Tsinghua University, Shenzhen 518055, China

^b School of Mechanical, Electronic and Control Engineering, Beijing Jiaotong University, Beijing 100044, China

^c School of Internet of Things Engineering, Jiangnan University, Wuxi 214122, China

^d Dalian Key Lab of Marine Micro/Nano Energy and Self-Powered Systems, Marine Engineering College, Dalian Maritime University, Dalian 116026, China

ARTICLE INFO

Keywords:

Ionic hydrogel
Strain-triboelectric sensors
Wearable skin
Underwater sensing
Soft robotic grasping

ABSTRACT

Hydrogel-based wearable devices and soft robotics have become a research hotspot. However, due to hydrogels' poor anti-dehydration and susceptibility to breakage, issues of recycling and waste stream contamination risks have severely limited large-scale applications. Moreover, the practical monitoring of robotic grasping is rather limited due to the complex underwater environment. In this work, an environment-friendly high-performance ionic hydrogel with fracture toughness (146.5 kJ/m^3) capable of strain and triboelectric sensing is developed. As a strain sensor, it owns good sensitivity (gauge factor: 4.30), a quick response time (70 ms), outstanding stability (~ 1000 cycles), low-temperature resistance, and well reproducibility (within one month). The hydrogel was also employed in the development of a flexible triboelectric sensor (200 % strain), which could respond sensitively to abundant types of materials (including water droplets). Due to these advantageous properties, the developed strain-triboelectric sensors can detect real-time human motion and grasping states of the soft gripper simultaneously. Thanks to the good degradability (~ 12 h), it may well address potential problems of high cost and risks during the underwater recycling process. To summarize, the developed all-in-one strain-triboelectric sensors have demonstrated great potentials in enhancing the actively perceiving capabilities during underwater soft robotic grasping.

1. Introduction

Recently, soft and stretchable electronics have received a lot of attention in overcoming the sensing and feedback control challenges faced by wearable electronics and soft robots [1–5]. Conductive hydrogels prepared by incorporating electronic conductive materials and ionic materials into polymer networks have extraordinary properties in terms of perception due to their designable conductivity, skin-matched Young's modulus (elastic modulus from 0.1 to 100 kPa) [6–12], and good compliance and biocompatibility [13]. However, electron-conductive materials such as conductive polymers [14], carbon-based materials [15], MXene [16], and metal-based materials commonly require the establishment of a second network for electron transfer due to the low conductivity of the tunneling effect at low concentrations, and their flexibility is also limited by rigid heterocyclic main chain structure [17,18]. In contrast, simple salt dissolution (NaCl,

CaCl₂ and LiCl, organic zwitterions, etc.) in hydrogel endows conductivity and can significantly lower the hydrogel's freezing point as well, which is widely used in strain sensors [19,20]. On the other hand, low-cost ionic hydrogels (IHs) merely change the configuration of water molecules and polymer networks during deformation, which has little effect on ionic conductivity [21]. As a result, they can be used as both the triboelectric layer and the flexible electrode in the application of triboelectric nanogenerators (TENG) [22,23]. TENG utilizes mechanically driven Maxwell displacement currents as the driving force, allowing for self-powered sensing by converting the environment's disordered and small (bio)mechanical excitations into electrical signals [24]. However, in practical applications, researchers had to encapsulate hydrogels to slow down their dehydration and improve durability. Although various hydrogels with adhesive, self-healing, and good environmental tolerance have been proposed [25–28], their excellent performance is achieved based on limited biocompatibility and

* Corresponding authors.

E-mail addresses: juntian.qu@sz.tsinghua.edu.cn (J. Qu), xuminyi@dmlu.edu.cn (M. Xu).

<https://doi.org/10.1016/j.nanoen.2023.108387>

Received 2 February 2023; Received in revised form 6 March 2023; Accepted 24 March 2023

Available online 25 March 2023

2211-2855/© 2023 Elsevier Ltd. All rights reserved.

environmental unfriendliness, even harmful to the body or the environment. As a result, when the encapsulation is damaged or at the end of its life [29,30], the recycling and disposal of hydrogels will seriously restrict its further practical development and widespread applications.

Due to a lack of suitable instruments, developing underwater salvage and marine resource management is exceedingly challenging [31]. Compared to traditional rigid manipulators, soft robotic hands can passively change shape and motion to adapt to a wide range of tasks, especially in interacting with unconventional objects, showing extraordinary advantages [32]. However, as sensory capabilities are the prerequisite for dexterous manipulation, soft robotic hands with infinite passive degrees of freedom pose a challenge to compatible sensors [33]. Zhang et al. [34] integrated the triboelectric sensor (TES) into the soft robotic gripper (SRG) to quantify the bending deformation state of SRG. Chen et al. [35] incorporated the TENG into the pneumatic soft actuator (PSA) as a configured proprioceptive sensor, and the output voltage of the TENG was linearly related to the total bending angle of the PSA. However, the limited flexibility of the sensing device (due to the demand of pairing with a particular actuator) has restricted its extensive applications. Considering the easy fabrication and flexible integration, Shen et al. [36] developed a hysteresis-free hydrogel-based strain sensor for soft gripper, whereas a single-mode sensor might lead to declined recognition accuracy, thus making the whole system unreliable [37]. In addition, some soft grippers made of hydrogel are still limited in perceptions of stable grasping or other grasping states [38–40], though capable of responding to surrounding stimuli. Ying et al. [41] reported a hydrogel-based ionic skin (iSkin) that can perform simple adhesion to enable grasping states' sensing of soft grippers. However, the significant and un-resolved issue is the post-possessing issue of the employed sensor once its service life is expired or is damaged. Transient electronic devices' components could be dissolved using a controlled manner after a period of operation [42]. This alternative is expected to provide a promising solution for mitigating environmental problems and eliminating the harm of e-waste. Polyvinyl alcohol (PVA)-xanthan gum (XG) has a wide range of applications in dust suppressant [43], water treatment [44], biodegradable food packaging material [45], and ecological friendly solid polymer electrolyte (SPE) matrices synthesis because of its good properties [46]. However, the investigation of sensing technologies based on PVA-XG has not been explored in depth.

To address the above challenges, we employed PVA and XG equipped with good degradation performance as the main materials and integrated them with glycerin (GL), glycerol, and NaCl in a one-pot method to develop an environment-friendly ionic hydrogel (PXGN IH) with high performance. The PXGN IH could be employed as a flexible strain sensor directly, and because of its stable ionic conductivity, it could also be assembled into a single-electrode mode TENG acting as a self-powered sensor. The main network's hydrogen bonds between PVA, XG, and GL were demonstrated with dominant mechanical properties (Young's modulus of 80 kPa and toughness of 146.5 kJ/m³). The strain sensor displays a good linear response ($R^2 = 0.996$) between relative resistance change and strain (gauge factor: 4.30) among the strain-sensing range of 0–200 %, possessing precise detection ability for both tiny movements and large deformations. The self-powered triboelectric sensor exhibits good stretchability and sensing performance. Silicone rubber material was selected as the triboelectric layer integrated with hydrogel, demonstrating sensitive responses upon contact with numerous materials. Finally, the developed strain-triboelectric sensors were incorporated into the two-finger soft robotic gripper in underwater robotic grasping, and precise grasping state and object slippage were perceived. In all, the developed all-in-one strain-triboelectric sensors pave the way for widespread applications of underwater soft robotic sensing.

2. Results and discussion

2.1. Fabrication and characterization of hydrogel

The strain-triboelectric sensors based on PXGN IH are designed for grasping state and object slippage monitoring, as illustrated in Fig. 1. Resistance is the work function of the strain sensor. The strain sensor deforms when the soft gripper grasps the object. According to the equation $R = \rho L/S$ (ρ is the resistivity of the strain sensor material, L is the length, and S is the cross-sectional area), when the strain sensor's material is determined, L and S change along with the altering of grasping state, thus the variation in resistance value directly represents the corresponding grasping state. Furthermore, the triboelectric sensor array was incorporated in the soft gripper, when the object slips, the external stimulation of the object may initiate the sensor's contact electrification process. This process can be explained using the electron-cloud-potential-well model [47,48]. The potential well prevents electrons from escaping before the object makes contact with the sensor array. When an object comes into contact with one of the arrays, the electron cloud of the positive and negative material overlaps, the energy barrier is decreased, and the electron is transferred, resulting in current flowing via the external circuit due to the formed potential difference. The time difference of the current (arrays) generated during the sliding process could be used to calculate the slip velocity. As a major component of the strain-triboelectric sensors, the PXGN IH was synthesized by incorporating NaCl into the composite hydrogel consisting of PVA, XG, and GL with the physically cross-linked synergistic network. NaCl was dissolved in GL and deionized water (DI). The hydrogen bond between GL and DI could prevent the formation of ice crystals and provide the hydrogel with good conductivity (Fig. 2a). The hydrogel intermediate was then produced by adding XG in a one-pot method at a high temperature, followed by the addition of PVA powder for intense mechanical mixing. Additionally, the ion-rich domain (as the electrical phase) ensures stable electrical properties for strain sensing, while the hydrogen-bonded cross-linked PVA, GL, and XG domains (as the mechanical phase) enable good mechanical stretching, as shown in Fig. 2b and c. The developed PXGN also owns high toughness, even a small piece of it ($3 \times 0.5 \times 0.2$ cm, 1 g) can readily lift 2 kg weight (Fig. 2d). The high-performance PXGN IH obtained by simple freeze-thawing has excellent environmental friendliness [40]. Degradability performance is crucial for hydrogel enabling its usage without additional expenses for recovery issues. To quantify the degradability, the swelling behavior of the hydrogel in water was investigated. Technically, measuring the degradation rate is the proper way to quantify biodegradability. Considering the degradation process of hydrogels in water cannot be intervened to obtain accurate degradation rates, we assessed the samples' degradability using qualitative observations. The dissolution rate of the hydrogel in water reached 100 % after ~ 5 h (Fig. S1a–f, Supporting information). This indicates that the hydrogel has strong degradability, being able to dissolve in water autonomously without the need for recycling. Considering that sodium chloride (NaCl) dissolved in water, when combined with water molecules, can form a hydration shell (salting effect), which not only changes the electrical conductivity of hydrogel but also has an effect on its mechanical properties. PXGN-n will be used to represent the hydrogel in this section, where n is the NaCl content. By repeating the above fabrication methods and altering the weight percent of NaCl to 0 wt%, 4.6 wt%, 5.7 wt%, and 6.8 wt%, respectively, four distinct hydrogels, designated PXGN-0, PXGN-4.6, PXGN-5.7, and PXGN-6.8, were created.

In Fig. 2e, the PXGN-5.7 reached a high tensile modulus of 137 kPa without fracture at a strain of 200 %. PXGN-0, PXGN-4.6, and PXGN-6.8 broke at lower tensile stresses of 30 kPa, 150 kPa, and 86 kPa (corresponding strains of 100 %, 150 %, and 300 %), from which PXGN-5.7's fracture strain is twice of PXGN-0's. From PXGN-4.6 to PXGN-5.7, it could be observed that the salting-out effect has enhanced the interaction between PVA-PVA and PVA-glycerol with a small amount of

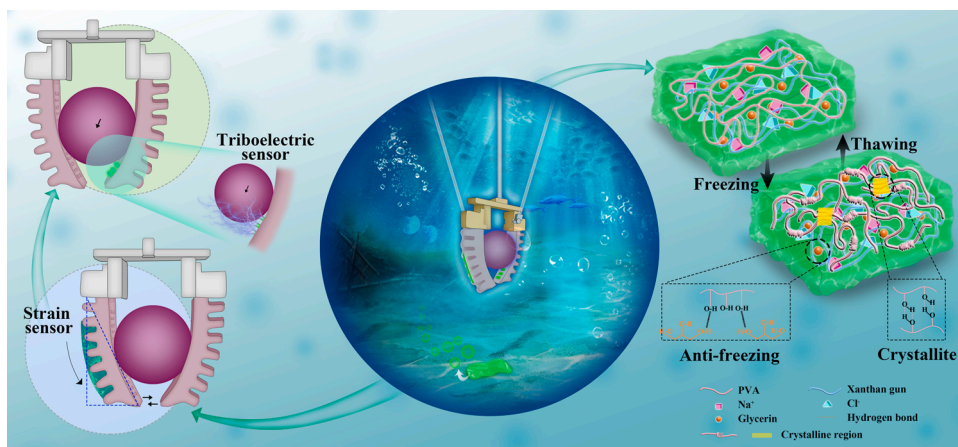


Fig. 1. Schematic illustration of a soft robotic gripper integrated with strain-triboelectric sensors based on the developed hydrogel and the formation mechanism of the hydrogel.

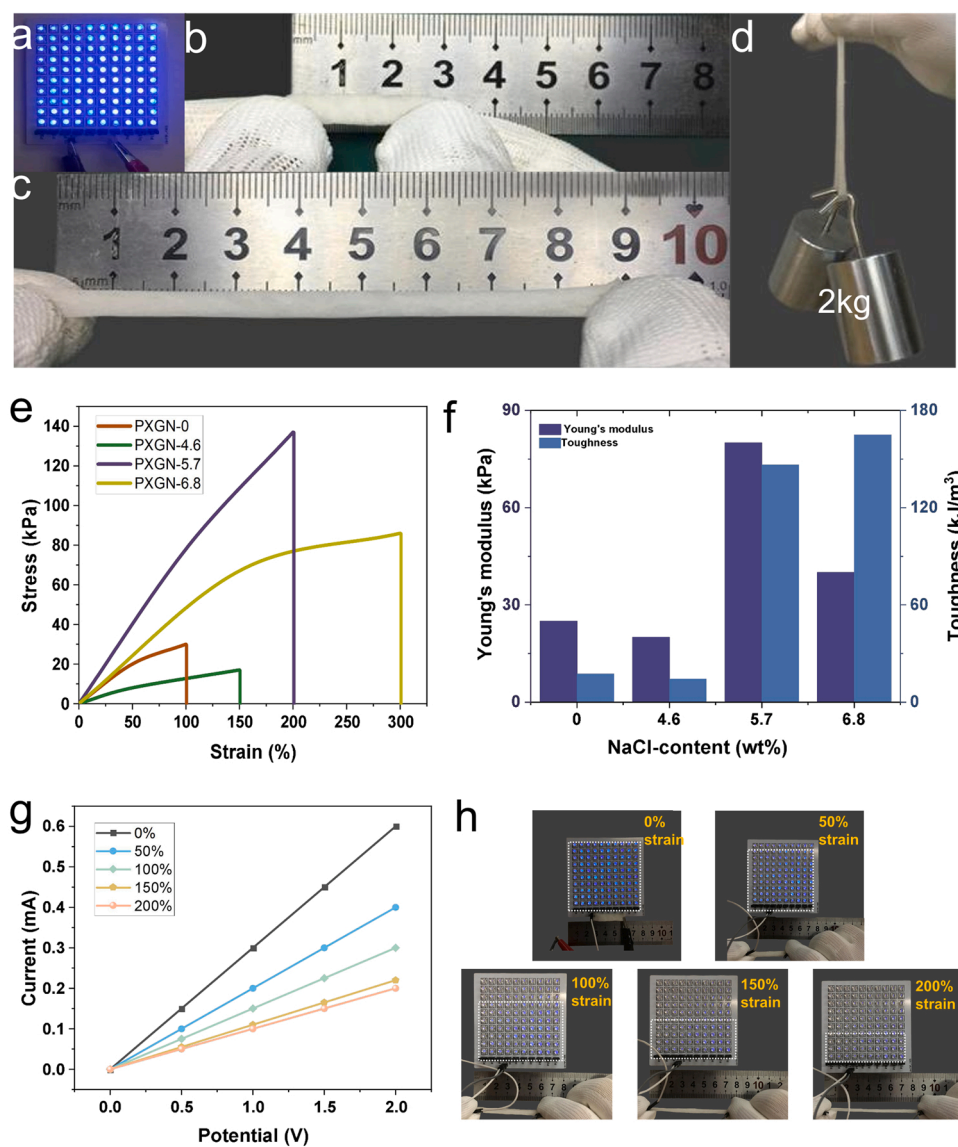


Fig. 2. Images of the PXGN hydrogel under tests of a) conducting, b-c) stretching, d) weightlifting, e) tension stress-strain curves, f) Young's modulus and toughness of PXGN hydrogel with different NaCl content. g) I-V curves of PXGN-5.7 hydrogel with different strains at 0–2 V, h) The change of LED luminance with the corresponding strain.

additional salt dissolved in the hydrogel [49]. From the graph, the PXGN-5.7 displays a modest fracture strain, but its Young's modulus (80 kPa) and toughness (146.5 kJ/m^3) (Fig. 2f) have been dramatically improved (compared with PXGN-0). PXGN-0, PXGN-4.6, and PXGN-6.8 own Young's modulus of 25 kPa, 20 kPa, and 40 kPa (corresponding toughness of 17.5 kJ/m^3 , 14.5 kJ/m^3 , and 165 kJ/m^3). Although PXGN-6.8 is tougher than PXGN-5.7 by 12.6 %, Young's modulus (40 kPa) is much lower (compared with 80 kPa). As a result, we determined that 5.7 wt% of NaCl additive in a hydrogel was the ideal amount. In order to better verify the interaction in the system, FTIR and XRD tests and analysis were made conducted on PXGN-5.7 (Fig. S2, Supporting information). At the same time, the PXGN-5.7 did not experience dehydration over one week (Fig. S3, Supporting information).

Besides, to verify the conductivity of PXGN-5.7, we connected the developed hydrogel with 100 LEDs. Fig. 2g shows the current-voltage (I-V) curves under different strains in the range of 0–2 V. It can be seen that the slope of the I-V curve decreases as the strain increases. From the equation $R = \rho L/S$ (ρ is the resistivity of the PXGN-5.7), as the S decreases, the L increases, leading to the gradual increase of the corresponding resistance (R) and darkening of the LEDs brightness (Fig. 2h).

2.2. Development of the hydrogel-based strain sensor

The hydrogel can be used as a strain sensor because of its good tensile and electrical conductivity. The performance of the hydrogel-based strain sensor is measured using the developed data acquisition experimental setup, which includes an electrometer and a linear motor (Video S1, Supporting information). Firstly, the hydrogel-based strain sensor shows a reliable response-ability to apply periodic load under different tensile conditions (Fig. 3a). The $\Delta R/R_0$ of the sensor increases significantly with enhanced tensile strain. In addition to high stretchability, the resistive response of the sensor can detect deformation as low as 0.3 mm ($\sim 1.0\%$ strain) as shown in Fig. 3b. Under low strain

conditions (1 %, 3 %, 5 %), the displayed sensing performance of the sensor is also reliable. In addition, the response time of the sensor was further evaluated (Fig. 3c), in which the loading and unloading times were tested to be 70 ms and 100 ms respectively. The gauge factor (GF) is a parameter representing the sensitivity of the sensor. In the range of 0–200 % strain, GF was calculated to be 4.30, as shown in Fig. 3d, where we can also observe good linearity ($R^2 = 0.996$) between the resistance change and the strain, demonstrating the uniformity of the developed hydrogel-based strain sensor. The hysteresis measured at the maximum strain value is 8 %, as shown in Fig. 3e. The sensor presents stable responses in 1000 tensile loading-unloading cycles (Fig. 3f left) at the strain of 80 %, indicating its excellent durability and repeatability during the long-term tension-release process. It should be noted that the sensor's durability and repeatability were checked again after one month (results shown in Fig. 3f right), and no apparent signal difference was observed. The several core parameters of the developed strain sensor are compared with other most advanced strain sensors, as shown in Table S1 (Supporting information). The sensor could detect human movement in a cold environment (Fig. S4a–b, Supporting information) and underwater environment (Video S2, Supporting information), and then we connected the hydrogel to a function generator (with a 20 Hz/10 V Voltage Peak-Peak) in series to activate 100 LEDs (Fig. S4c, Supporting Information). At both low temperatures and room temperature, it was observed that the lamp's brightness barely changed (Fig. S4d–e, Supporting information). This demonstrates that the developed sensor's sensitivity and decoupling capabilities remain strong even at low temperatures. These exceptional sensing performances have indicated the developed hydrogel-based strain sensor's great potential in practical applications such as wearable and electronic skin.

Supplementary material related to this article can be found online at [doi:10.1016/j.nanoen.2023.108387](https://doi.org/10.1016/j.nanoen.2023.108387).

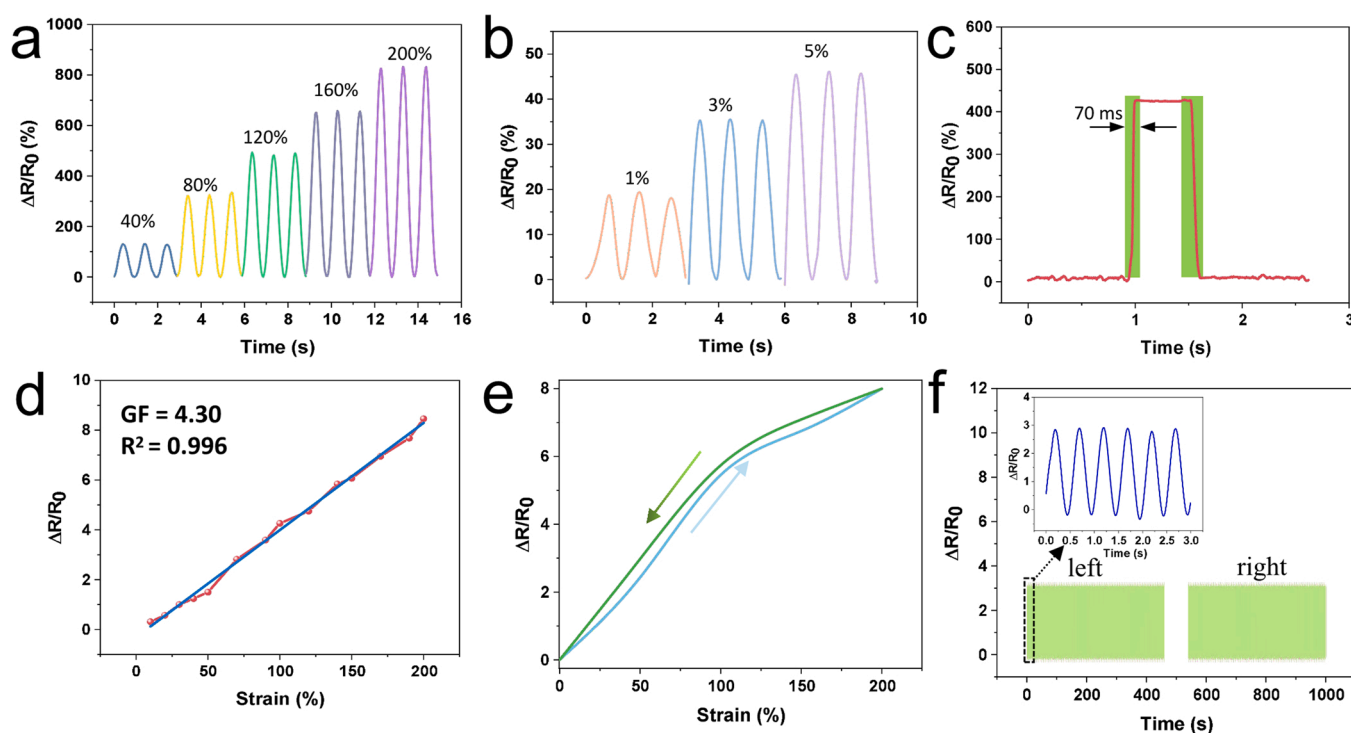


Fig. 3. Sensing properties of the strain sensor based on PXGN-5.7. a) Resistance response of the strain sensor stretched to different strains. b) Resistance response of the strain sensor under small strains (1 %, 3 %, and 5 %). c) Response time of the hydrogel-based strain sensor. d) Relative resistance changes of the sensor as a function of applied strain (0–200 %). e) Hysteresis curve of the strain sensor at maximum strain. f) Cycling stability test at the strain of 80 %. The top inset shows the beginning 6 cycles, the bottom left inset shows the relative resistance changes curve within 1000 cycles, bottom right inset shows relative resistance changes after one month.

2.3. Development of the hydrogel-based triboelectric sensor

With the hydrogel as the electrode, a single-electrode-mode triboelectric sensor (area: $1.5 \times 1.5 \text{ cm}^2$) was fabricated (Fig. 4a). The silicone rubber dielectric layer (250 μm thickness, selected based on systematic investigation results shown in Fig. S5 of Supporting information) serves as the top triboelectric layer of the sensor. The working mechanism of a triboelectric sensor is based on the coupling effect of triboelectrification and electrostatic induction. When the top dielectric layer (silicone rubber) contacts with the external object, it generates equivalent amounts of opposite charges at the two layers' surface (Fig. 4b (i)). When the external object is separated from the dielectric layer, the electrostatic charges on the surface of the top dielectric layer will drive the ions of hydrogel to the interface, generating a layer of positive ions to balance the electrostatic charge. At the same time, the interface of copper wire and hydrogel will be polarized, thus forming the same amount of negative ions at the interface of copper wire and

hydrogel, then the electrons will flow along the copper wire to the ground (Fig. 4b (ii)) until the object is completely departed away from the top dielectric layer (Fig. 4b (iii)). Finally, when the object approaches the top dielectric layer once again, electrons will flow back through the external circuit to the copper wire and the hydrogel interface (Fig. 4b (iv)). Fig. 4c presents the COMSOL Multiphysics simulation result verifying a great potential difference between the object skin and the silicone rubber layer (top dielectric layer). The continuous contact-separation motion will result in continuous power, and its quarter-cycle simulation voltage curve is shown in Fig. S6a-d (Supporting information). To note, the abovementioned external object can be made of enormous types of materials, as presented in Fig. 4d (variant voltage responses to different types of materials at the same 1 Hz, 20 cm test conditions), demonstrating the universality of the developed TENG sensor in multiple scenarios.

We assessed the stretchability of the triboelectric sensor (3 cm \times 0.5 cm) adopting a tensile test. The triboelectric sensor was

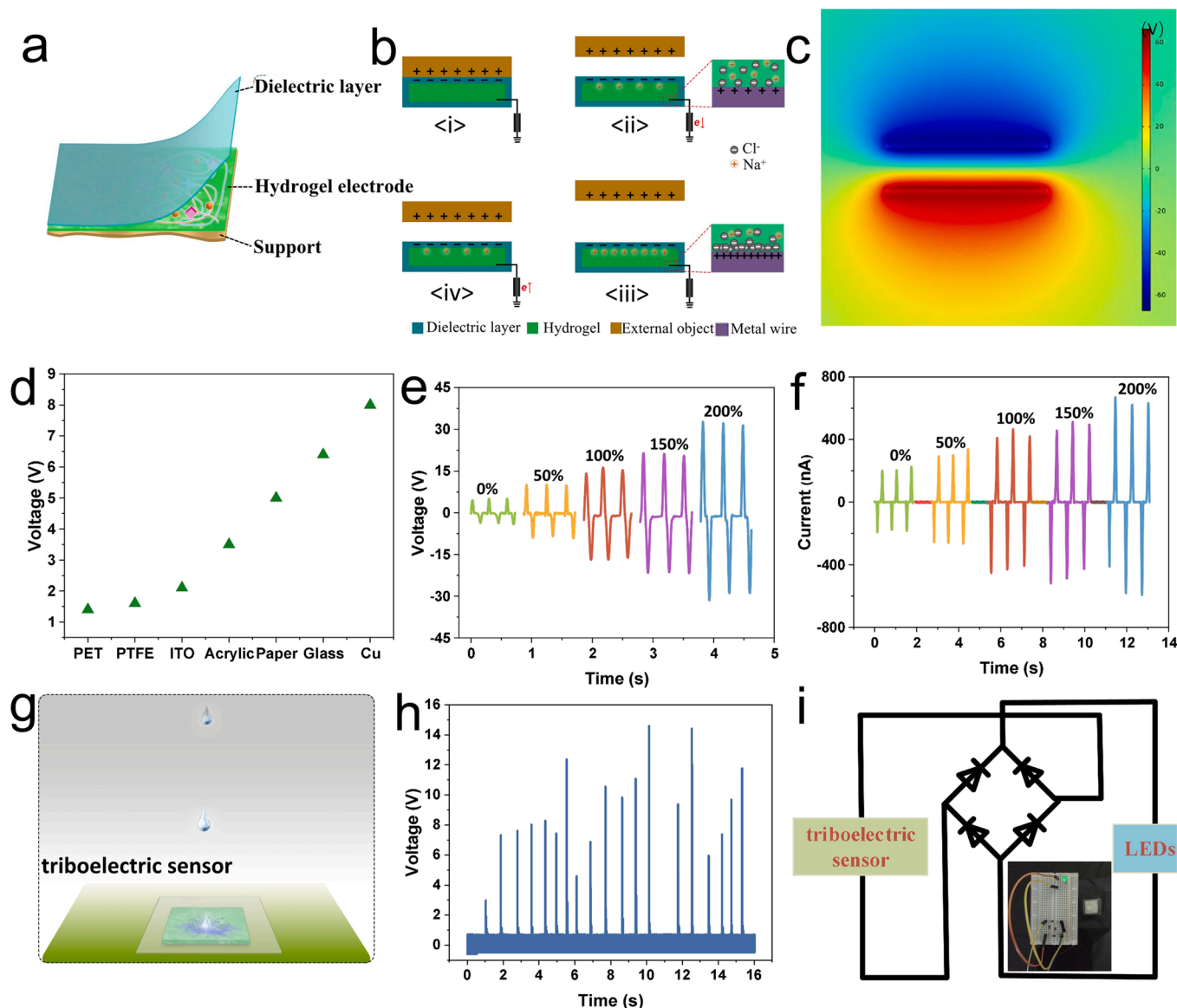


Fig. 4. Operating principles and electrical output performance of the hydrogel-based triboelectric sensor. a) Structural schematic of the triboelectric sensor. b) schematic working principle of the triboelectric sensor. c) Finite element simulation of potential distribution to illustrate the operation mechanism of the triboelectric sensor. d) Open-circuit voltage by replacing other external objects. e) Open-circuit voltage, and f) short-circuit current as a function of stretched length. g) Schematic diagram of water droplets impacting the triboelectric sensor. h) The output voltage of the triboelectric sensor when it is impacted by water droplets of different states. i) The lighten-up LED under the impact of the water droplet.

uniaxial stretched to different strains, and the corresponding electrical voltage output was recorded during periodic contact-separation motions (Fig. 4e, f). After being stretched by 50–200 %, the open circuit voltage of the triboelectric sensor was dramatically increased from ~ 10 V to ~ 30 V, and the corresponding short circuit current was significantly enhanced from ~ 200 nA to ~ 600 nA, which could be attributed to the enlarged TENG sensor's surface area in the tensile condition.

The presented hydrogel-based triboelectric sensor also possesses good hydrophobicity. In our test, it could transform the impact force (produced by the falling water droplets) into electrical signals (Fig. 4g and Video S3, Supporting information) when the droplets were ejected from a syringe above the triboelectric sensor (Fig. 4h). When the height was increased from 20 cm to 50 cm, the sensor's output voltage was enhanced from 5 V to 14 V (Fig. S7, Supporting information). And in order to further measure the output performance of the triboelectric sensor as a self-powered system, the led can be obviously lit through the rectifier circuit (Fig. 4i). The above experimental results demonstrate that triboelectric sensors could serve as an optical indicator in waterproof-detection applications. Moreover, the triboelectric sensor remains stable voltage output under the influence of variant magnetic fields (Fig. S8, Supporting information).

Supplementary material related to this article can be found online at [doi:10.1016/j.nanoen.2023.108387](https://doi.org/10.1016/j.nanoen.2023.108387).

2.4. Demonstration as dual-mode hydrogel-based wearable skin

Self-powered smart skin can help robots perceive the surrounding environmental information without the need for an additional power supply. We developed a wearable strain-triboelectric sensor skin (STSS)

based on hydrogel. To equip the STSS with the ability of spatial mapping towards external stimuli, in our design, a silicone film (area: $3.5\text{ cm} \times 3.5\text{ cm}$) was attached to seven pieces of developed hydrogel pads (schematically shown in Fig. S9, Supporting information). In the array, pad ST-4 (area: $1\text{ cm} \times 3\text{ cm}$) was designed for both strain sensing and triboelectric sensing tasks, while the remaining six hydrogel pads (unit area: $1\text{ cm} \times 1\text{ cm}$) were designed for sole triboelectric sensing (Fig. 5a). The wrist-mounted STSS can precisely identify the contact point, as illustrated in Figs. 5b and 5c. The voltage outputs of three pads (ST-4, 5, and 7) are at consistent levels (a similar compressive force was applied by each finger) because of identical surface area. In particular, the ST-4 sensor can be employed to determine the contact area (finger numbers) between an external object and the STSS (Fig. S10, Supporting information). We tapped the ST-4 with our fingers (under a similar force level) along its length direction, as the contact area increased from one finger to three fingers, the output voltage was doubled and tripled gradually (corresponding voltage increases from ~ 2 V to ~ 6 V). Fig. 5d depicts the output voltage as the finger moves across the seven STSS unit pads on a specific trajectory, with a detection resolution of 10 mm and spacing of 3 mm (Fig. 5e). The sliding speed can be calculated based on the time interval between adjacent peaks, a shorter time interval indicates a faster sliding speed. To better understand the output performance of STSS during sliding, finite element analysis was used to obtain the voltage distribution at different contact locations of a certain STSS unit (Fig. S11, Supporting information). When the wrist is bent 90° back and forth (Fig. 5f), the resistance of ST-4 changes $\sim 1\text{ k}\Omega$, in which consistent output demonstrated stable performance of STSS.

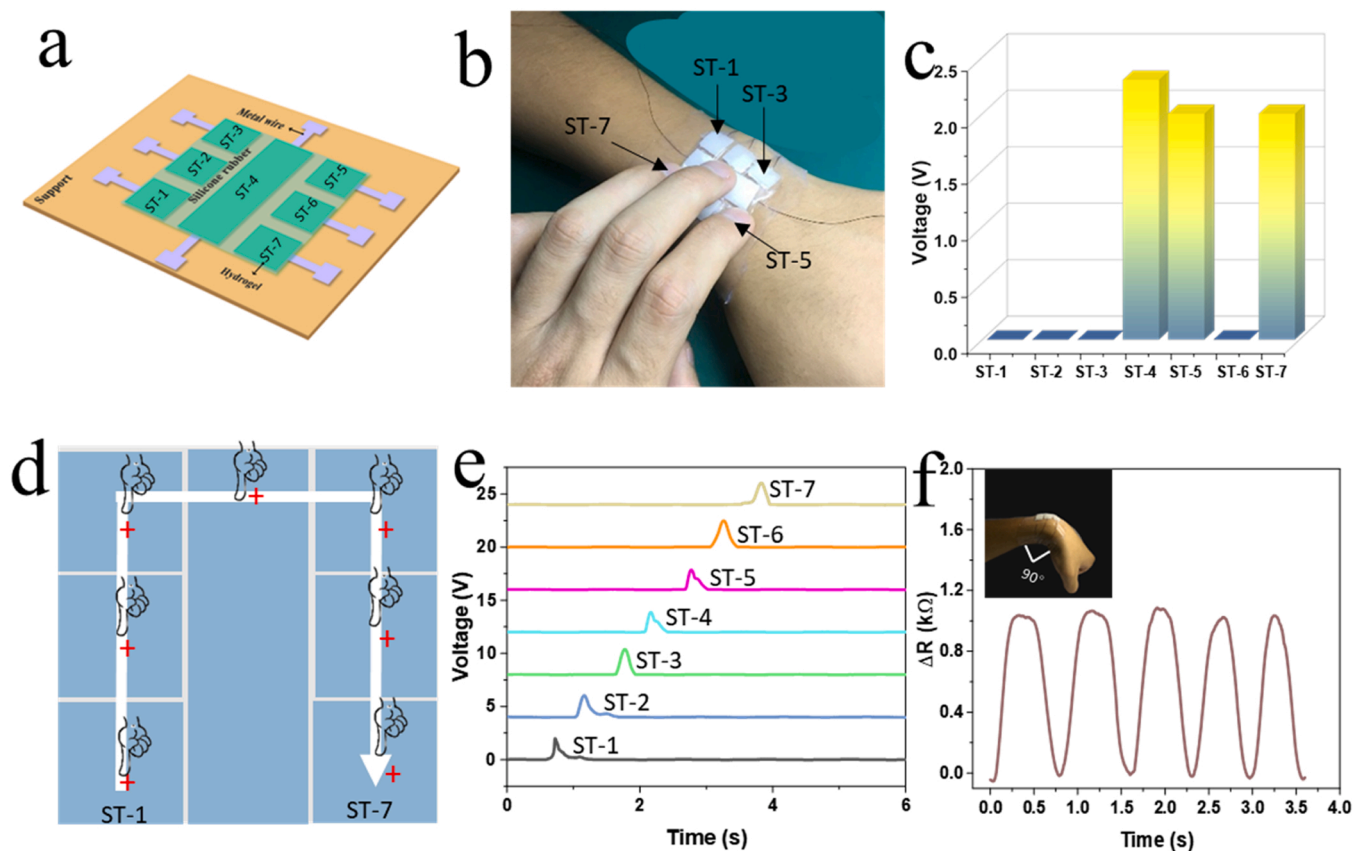


Fig. 5. Development of wearable strain-triboelectric sensor skin (STSS). a) 3D schematic layout design of the wearable STSS. b) A Photograph of the STSS mounted on the wrist with a three-finger touch c) Spatial mapping results. d) Schematic description of a finger moving over the STSS surface and e) Corresponding spatial mapping in terms of voltage. f) Real-time relative resistance changes of the strain sensor unit for human motion detection, the top inset shows the image of STSS being worn on the wrist.

2.5. Underwater robotic grasping detection based on strain-triboelectric sensors

The good degradability and environment-friendly properties of PXGN IH endow it with great potential for sensing in the underwater environment. Hydrogel-based strain-triboelectric sensors were attached to the soft gripper's surface (Fig. 6a). When the gripper was bent, the feedback strain data could help to determine the grabbed object's size and grasping state. Due to the complexities of the pneumatic gripper's strain, the bending angle (θ) was recorded to reflect the strain. With a gradual increase of pneumatic pressure from 0 kPa to 200 kPa, the grippers could autonomously perceive the bending angle. The objects to be clamped were classified into three categories based on the resistance response of the attached sensor. Varying air pressures were configured for size sorting based on corresponding resistance responses ($\Delta R/R_0$), as shown in Fig. 6b, small size object (resistance responses < 0.2), medium

size object ($0.2 \leq$ resistance responses ≤ 0.4), and large size object (resistance responses > 0.4) are classified, respectively.

In practical underwater object grasping, accidental interference, slippage, or collision may lead to grasping failure or even damage to the gripper. As a result, unstable robotic grasping detection is the first step in the designed grasping strategy. Three hydrogel-based triboelectric sensors (top sensor: TENG-Ch1, middle sensor: TENG-Ch2, bottom sensor: TENG-Ch3) were integrated (as an array) into the lower grooves of the gripper's inner surface. It is worth noting that when the triboelectric sensors were utilized underwater, the operating principle was illustrated following the protocol illustrated in Fig. S12 (Supporting information). In addition, we have encapsulated the sensors (with PTFE tape), which not only avoids underwater charge dissipation issue on the triboelectric sensors array but also ensures longer time of normal operation. As the object slides along the triboelectric sensors array, the contact between the silicon film layer and the hydrogel electrode layer

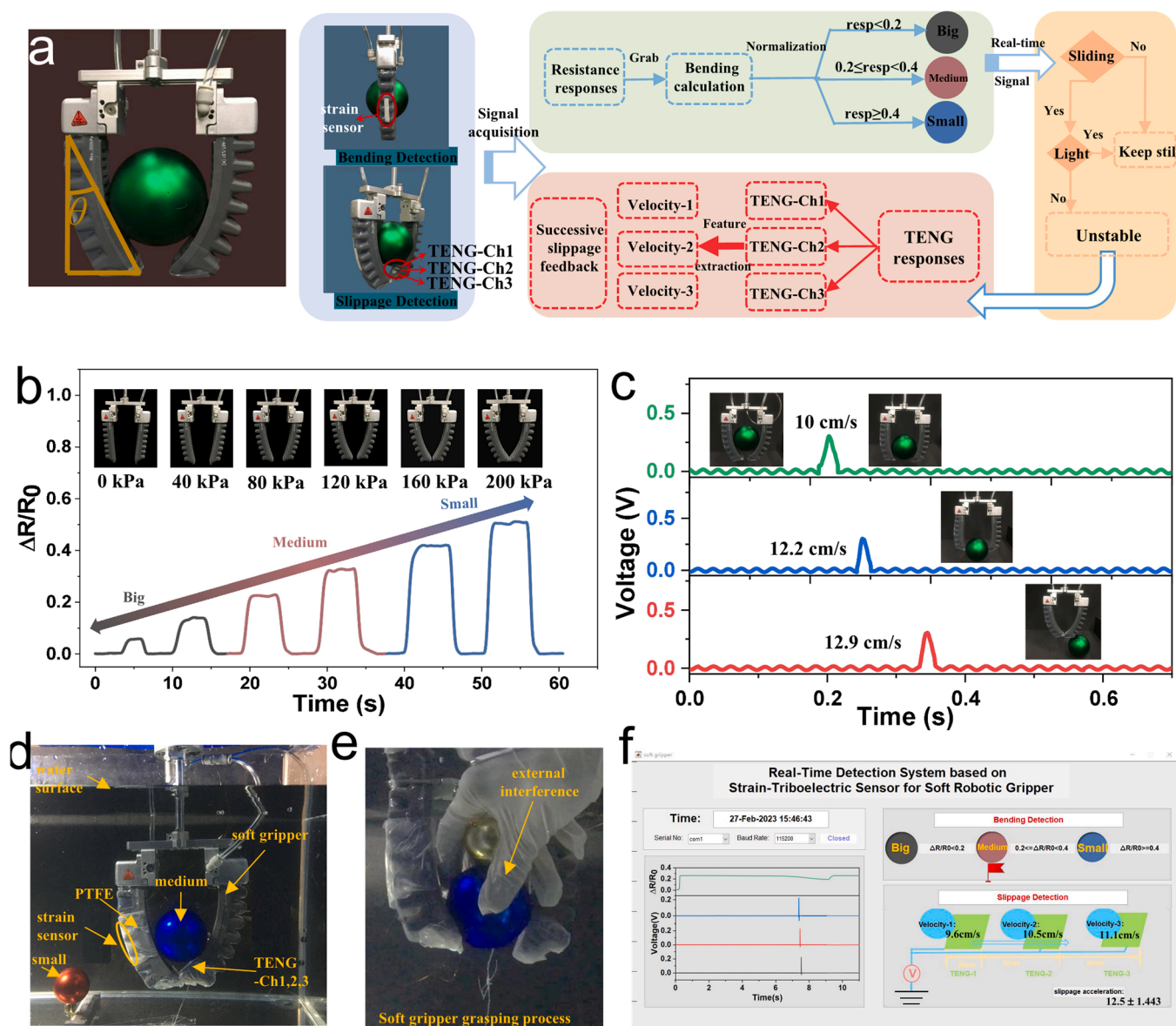


Fig. 6. Real-time detection for the soft robotic gripper. a) Photograph of two-finger pneumatic soft grippers and the sensing framework, which is capable of grasping objects with different radiuses and reflecting the grasping state. b) The defined bending angles θ correspondingly increase. Relative change in resistance as the pneumatic pressure gradually increases. The insets show the front-view photographs of the gripper under different pressure conditions. c) Slippage test. The insets show the front-view photographs of the gripper under the ball slides through the triboelectric sensor array. d) Photograph of the robotic soft gripper integrated with strain-triboelectric sensors for underwater grasping of spherical objects. e) Photograph of underwater grasping encountered with external interference. f) Real-time detection interface for underwater grasping based on strain-triboelectric sensors.

may change the local electric field distribution, leading to electron transfer between the electrode and the ground, hence, an external circuit with a positive current signal peak could be detected.

To test the feasibility of slippage detection, a ball was controlled to slide downwards along the soft gripper during grasping, and the interval between each array unit is set at 3 mm. The average velocity could be calculated using based on the well-known formula: $v = \Delta d / \Delta t$, additionally, according to the acceleration formula: $a = \Delta v / \Delta t$, where Δt refers to the time from the object sliding out of the previous array to the contact with the next array. Thus, the sliding acceleration could be calculated as $12.5 \pm 1.443 \text{ mm/s}^2$ (Fig. 6c, Fig. S13a, Supporting information).

A real-time slippage detection system was developed to demonstrate the prospects of the soft gripper in intelligent perception and control. The system is capable of underwater grasping monitoring (Fig. 6d), which is significant for safe/stable grasping in case of visual failure/difficulty in the underwater environment. As shown in Fig. 6e, when a ball is grasped by the soft gripper, the hydrogel-based strain sensor will detect the change of bending state, and the hydrogel-based triboelectric sensors can simultaneously monitor slippage for the grasped object, during which process (Video S4), we can observe that resistance and voltage responses are low at the initial stage. As the grasped ball approached the soft gripper, the resistance responses begin to rise while the voltage remains unchanged because there was no sliding occurred between the ball and the grippers. When the sliding process encountered an external collision, resistance responses fell slightly whereas the three triboelectric sensors responded instantly generating three sequential voltage peak signals (velocity 1: 8.57 cm/s, velocity 2: 9.09 cm/s and velocity 3: 10 cm/s, corresponding resistance changes was low due to slight deformation). When the ball was pushed out of the gripper finger completely, the gripper's bending degree and resistance responses returned to the initial grasping state due to the constant air pressure. As shown in Video S4, besides resistance and voltage peak curves displays, the determination of object size, real-time sliding speed, and sliding acceleration speed could all be presented in the user interface of the developed slippage detection system. The sliding acceleration of linear fitting is calculated to be $20.967 \pm 3.667 \text{ mm/s}^2$ (Fig. S13b, Supporting information). Additionally, it is observed that the sensing results of strain-triboelectric sensors are consistent in mediums of seawater and freshwater (Table S2, Supporting information). This practical slippage detection demonstration has illustrated the great potential of the developed dual-mode hydrogel-based sensors in intelligent underwater perception and robotic manipulation applications.

Supplementary material related to this article can be found online at [doi:10.1016/j.nanoen.2023.108387](https://doi.org/10.1016/j.nanoen.2023.108387).

3. Conclusion

In this work, we reported the design and characterization of ionic PXGN hydrogel and demonstrated its applications as all-in-one strain-triboelectric sensors for wearable sensing and soft robotics. The hydrogel owns good degradability (~ 12 h), avoiding problems of high recovery costs and waste logistics pollution risk during the underwater recycling process. The PXGN-5.7 has a toughness of 146.5 kJ/m^3 , which allows it to sustain a 200 % strain without breaking. In this first sensing mode, the hydrogel-based strain sensor has excellent stability (1000 times), a quick response time (70 ms), low hysteresis (8 %), high sensitivity (gauge factor: 4.30), and a fast recovery time (100 ms). In addition, the sensitive resistance response of the developed hydrogel-based strain sensor can detect deformation as low as 0.3 mm (~ 1.0 % strain). In another sensing mode, the hydrogel was also employed in the development of a flexible triboelectric sensor, which could respond sensitively to abundant types of materials (especially, water droplets impact was investigated). As shown in the first practical demonstration, the developed dual-mode hydrogel-based wearable skin presents a delicate perception of wrist movement and touch position. Finally, in the

second demonstration, by incorporating the developed strain-triboelectric sensors into the underwater soft gripper, the real-time unstable states (accidental interference, slippage, or collision) could be detected timely preventing failure grasping, which is expected to enhance the sensing capabilities and success rate of underwater soft robotic grasping.

4. Experimental section

4.1. Materials

PVA 1788 (alcoholysis degree 99 %), Gum xanthan ((C35H49O29)_n, viscosity (1 %KCl)mPa.s ≥ 1200 , Purity ≥ 99 %), 1,2,3-Propanetriol, Glycerin (content : 99.9 %), Sodium chloride; Halite (content : ≥ 99.5 % (AT)) was supplied by Hefei QASEG Co., Ltd, deionized water (resistivity $\geq 1 \text{ M}\Omega \text{ cm}$) were used in the experiment, Dow Corning 3140 RTV (room temperature vulcanized silicone rubber, elongate: 419 %, Dissipation factor (dielectric loss angle) (100 Hz): 0.004) were purchased from Beijing Branch, Du Pont China Holding Co., Ltd. Indium tin oxide (ITO, base material: polyester film, surface resistance: 10Ω) were purchased from Langu Electronic Technology Co., Ltd. Polytetrafluoroethylene (PTFE) VHB were purchased from Taobao.

4.2. Synthesis of ionic hydrogel

Sodium chloride (5.7 wt%) was added to a solvent mixture of deionized water (26 mL) and glycerol (8 mL) and vigorously stirred until completely dissolved. Xanthan gum (0.6 g) was added to the mixed solution and stirred at $80 \text{ }^\circ\text{C}$ for about 0.5 h until all of the powders were dissolved, obtaining a xanthan gum solution (1.5 wt%). PVA (4 g) should be divided into 10 sections, each of which should be added after the first 0.4 g has completely dissolved. The mixture should then be vigorously stirred at $100 \text{ }^\circ\text{C}$ for an hour to ensure that all the PVA has dissolved. Finally, place the mold in a temperature range of $-22 \text{ }^\circ\text{C}$ to $-20 \text{ }^\circ\text{C}$. After 12–14 h, remove the mold from the refrigeration equipment and defrost it for 1 h, then repeat the freezing and thawing process three times.

4.3. Fabrication of hydrogel-based strain sensor

Two copper wires are inserted into both ends of the hydrogel as electrodes to conduct resistance signals. When conducting wearable sensing and underwater soft robotic grasping, a layer of silicone rubber is covered on top of hydrogel to serving as dielectric layer (triboelectric sensor) and immobilizing the hydrogel layer. The liquid rubber (Dow Corning 3140 RTV, Du Pont China Holding Co., Ltd) was plated by a glass coating table and an SZQ Wet film preparator (thickness, $250 \pm 3 \mu\text{m}$). Then waiting for 1 h at room temperature for the liquid to become a thin elastomer.

4.4. Fabrication of hydrogel-based triboelectric sensor

Triboelectric sensor has a two-layer design. The silicone rubber serves as the top layer, with the hydrogen layer beneath it. Fix the ITO substrate surface upward on the glass coating platform, apply 3140 RTV silicone rubber to the ITO substrate surface, and use a four-sided coating preparation device to apply the silicone rubber to $250 \mu\text{m}$. The copper wire is inserted into the hydrogel during the experiment. In addition, when applying the triboelectric sensor to the gripper, making a 1 mm gap between silicone rubber and hydrogel to ensure that the triboelectric positive material is a silicone film, the hydrogel is used as both a negative triboelectric material and a conductive electrode, and the PTFE tape was selected for the sealing task.

4.5. Characterization and measurements

The Fourier transform infrared (FTIR) spectrum of a hydrogel in the range of 4000–400 cm^{-1} recorded using the attenuated total reflectance (ATR) method on Thermo Fisher Nicolet Is5. The X-ray diffraction (XRD) of the hydrogel by X-ray diffractometer (Rigaku Ultima IV, Japan). Data in the range of 5–90 degrees were recorded at ambient temperature using 40KV and 40 mA Cu K α radiation. At room temperature, through the stretching machine (ETM105D-TS 100 kN, Shenzhen Wance Technologies Co., LTD) at the tensile speed of 100 mm min^{-1} . Young's modulus and toughness are estimated from the slope of the stress-strain curve (5–20 % strain) and the area below the curve, respectively. The hysteresis energy is calculated according to the area enclosed by the load-unload curve, $\text{DH} = (|A_L - A_U|/A_L) \times 100\%$ as the average degree of hysteresis (DH), where A_L and A_U are the areas under loading and unloading curves, respectively. A function generator (TFG6940G, 40 MHz) was used to verify conductivity by lighting LEDs in series with the hydrogel. The strain sensor characteristics were tested by a linear motor (LQ-235, Beijing) with variable stretching frequency and displacement, and the resistance signal of the strain sensor was measured by an electrometer (Keithley-6514, USA). The strain sensor was repeatedly pre-stretched and relaxed for approximately 100 cycles to stabilize the electrical properties before long-term cycling tests. The GF is characterized by $(\Delta R/R_0)/\delta$, where R_0 and ΔR are the initial resistance and resistance change when the strain δ is applied, respectively. The multiplexed electrical signals of the STSS and the flexible gripper are processed by Origin (OriginLab Corporation). The soft gripper (Suzhou Soft Touch Robot Technology Co., LTD) is fixed to the end of an industrial robot (UR5, Universal Robots (Shanghai) Co., LTD) to perform gripping tasks. MSO44 (Tektronix) and electrometer are mainly used to measure voltage. Data collection and analysis were performed utilizing the LabVIEW software platform. The final real-time monitoring system was designed through the MATLAB Graphical User Interface (MathWorks, USA) program.

4.6. Informed consent statement

The described tests on humans do not require institutional review board (IRB) approval because these experiments do not affect the body or physiology of living humans, and all participants are authors of this paper who participated after giving informed consent.

CRedit authorship contribution statement

Juntian Qu: Supervision, Conceptualization, Methodology, Writing – original draft, Funding acquisition. **Qiangjing Yuan:** Methodology, Data curation, Writing – original draft. **Zhenkun Li:** Writing – review & editing. **Ziqiang Wang:** Writing – review & editing. **Feng Xu:** Writing – review & editing. **Qigao Fan:** Writing – review & editing. **Min Zhang:** Writing – review & editing. **Xiang Qian:** Writing – review & editing. **Xueqian Wang:** Writing – review & editing. **Xiaohao Wang:** Writing – review & editing. **Minyi Xu:** Supervision, Conceptualization, Methodology, Writing – original draft, Funding acquisition.

Declaration of Competing Interest

The authors declare that they have no known competing financial interests or personal relationships that could have appeared to influence the work reported in this paper.

Data Availability

Data will be made available on request.

Acknowledgments

This work was supported by the National Natural Science Foundation of China (Grant no. 52103283), the Shenzhen “Pengcheng Peacock Program”, the Beijing “Youth Talent Promotion Project”, the Tsinghua SIGS Cross-disciplinary Research and Innovation Fund (Grant no. JC2022002), and the Tsinghua SIGS Scientific Research Startup Fund (Grant no. QD2022021C). The corresponding author Minyi Xu acknowledges the financial support from the Dalian Outstanding Young Scientific and Technological Talents Project (2021RJ11).

Appendix A. Supporting information

Supplementary data associated with this article can be found in the online version at [doi:10.1016/j.nanoen.2023.108387](https://doi.org/10.1016/j.nanoen.2023.108387).

References

- [1] X. Zhang, C. Cui, S. Chen, L. Meng, H. Zhao, F. Xu, J. Yang, Adhesive ionohydrogels based on ionic liquid/water binary solvents with freezing tolerance for flexible ionotronic devices, *Chem. Mater.* 34 (2022) 1065–1077, <https://doi.org/10.1021/acs.chemmater.1c03386>.
- [2] Y. Yang, S. Duan, H. Zhao, Advances in constructing silver nanowire-based conductive pathways for flexible and stretchable electronics, *Nanoscale* 14 (2022) 11484–11511, <https://doi.org/10.1039/D2NR02475F>.
- [3] V. Orts Mercadillo, K.C. Chan, M. Caironi, A. Athanassiou, I.A. Kinloch, M. Bissett, P. Cataldi, Electrically conductive 2D material coatings for flexible and stretchable electronics: a comparative review of graphenes and MXenes, *Adv. Funct. Mater.* 32 (2022) 2204772, <https://doi.org/10.1002/adfm.202204772>.
- [4] H. Song, G. Luo, Z. Ji, R. Bo, Z. Xue, D. Yan, F. Zhang, K. Bai, J. Liu, X. Cheng, W. Pang, Z. Shen, Y. Zhang, Highly-integrated, miniaturized, stretchable electronic systems based on stacked multilayer network materials, *Sci. Adv.* 8 (2022) eabm3785, <https://doi.org/10.1126/sciadv.abm3785>.
- [5] G. Lee, M. Zarei, Q. Wei, Y. Zhu, S.G. Lee, Surface wrinkling for flexible and stretchable sensors, *Small* 18 (2022) 2203491, <https://doi.org/10.1002/sml.202203491>.
- [6] Z. Xu, Y. Han, Y. Bai, X. Chen, J. Guo, L. Zhang, C. Gong, Q. Luo, T. Zhang, C.-Q. Ma, Thermoplastic elastomer enhanced interface adhesion and bending durability for flexible organic solar cells, *Npj Flex. Electron.* 6 (2022) 56, <https://doi.org/10.1038/s41528-022-00188-2>.
- [7] C. Zhou, T. Wu, X. Xie, G. Song, X. Ma, Q. Mu, Z. Huang, X. Liu, C. Sun, W. Xu, Advances and challenges in conductive hydrogels: from properties to applications, *Eur. Polym. J.* 177 (2022), 111454, <https://doi.org/10.1016/j.eurpolymj.2022.111454>.
- [8] G. Li, C. Li, G. Li, D. Yu, Z. Song, H. Wang, X. Liu, H. Liu, W. Liu, Development of conductive hydrogels for fabricating flexible strain sensors, *Small* 18 (2022) 2101518, <https://doi.org/10.1002/sml.202101518>.
- [9] R. Tong, G. Chen, D. Pan, H. Qi, R. Li, J. Tian, F. Lu, M. He, Highly stretchable and compressible cellulose ionic hydrogels for flexible strain sensors, *Biomacromolecules* 20 (2019) 2096–2104, <https://doi.org/10.1021/acs.biomac.9b00322>.
- [10] J. Lee, M.W.M. Tan, K. Parida, G. Thangavel, S.A. Park, T. Park, P.S. Lee, Water-processable, stretchable, self-healable, thermally stable, and transparent ionic conductors for actuators and sensors, *Adv. Mater.* 32 (2020) 1906679, <https://doi.org/10.1002/adma.201906679>.
- [11] Z. Chen, J. Liu, Y. Chen, X. Zheng, H. Liu, H. Li, Multiple-stimuli-responsive and cellulose conductive ionic hydrogel for smart wearable devices and thermal actuators, *ACS Appl. Mater. Interfaces* 13 (2021) 1353–1366, <https://doi.org/10.1021/acami.0c16719>.
- [12] F. Fu, J. Wang, H. Zeng, J. Yu, Functional conductive hydrogels for bioelectronics, *ACS Mater. Lett.* 2 (2020) 1287–1301, <https://doi.org/10.1021/acsmaterialslett.0c00309>.
- [13] H.C. Yu, X.P. Hao, C.W. Zhang, S.Y. Zheng, M. Du, S. Liang, Z.L. Wu, Q. Zheng, Engineering tough metallosupramolecular hydrogel films with kirigami structures for compliant soft electronics, *Small* 17 (2021) 2103836, <https://doi.org/10.1002/sml.202103836>.
- [14] N. K, C.S. Rout, Conducting polymers: a comprehensive review on recent advances in synthesis, properties and applications, *RSC Adv.* 11 (2021) 5659–5697, <https://doi.org/10.1039/D0RA07800J>.
- [15] J. Anjali, V.K. Jose, J.-M. Lee, Carbon-based hydrogels: synthesis and their recent energy applications, *J. Mater. Chem. A* 7 (2019) 15491–15518, <https://doi.org/10.1039/C9TA02525A>.
- [16] Y. Zhang, M. Gong, P. Wan, MXene hydrogel for wearable electronics, *Matter* 4 (2021) 2655–2658, <https://doi.org/10.1016/j.matt.2021.06.041>.
- [17] F. Wahid, X.-J. Zhao, S.-R. Jia, H. Bai, C. Zhong, Nanocomposite hydrogels as multifunctional systems for biomedical applications: current state and perspectives, *Compos. Part B: Eng.* 200 (2020), 108208, <https://doi.org/10.1016/j.compositesb.2020.108208>.
- [18] H. Sun, Y. Zhao, C. Wang, K. Zhou, C. Yan, G. Zheng, J. Huang, K. Dai, C. Liu, C. Shen, Ultra-stretchable, durable and conductive hydrogel with hybrid double network as high performance strain sensor and stretchable triboelectric

- nanogenerator, *Nano Energy* 76 (2020), 105035, <https://doi.org/10.1016/j.nanoen.2020.105035>.
- [19] L.G. Greca, J. Lehtonen, B.L. Tardy, J. Guo, O.J. Rojas, Biofabrication of multifunctional nanocellulosic 3D structures: a facile and customizable route, *Mater. Horiz.* 5 (2018) 408–415, <https://doi.org/10.1039/C7MH01139C>.
- [20] R. Guo, Y. Fang, Z. Wang, A. Libanori, X. Xiao, D. Wan, X. Cui, S. Sang, W. Zhang, H. Zhang, J. Chen, Deep learning assisted body area triboelectric hydrogel sensor network for infant care, *Adv. Funct. Mater.* 32 (2022) 2204803, <https://doi.org/10.1002/adfm.202204803>.
- [21] L. Tang, S. Wu, J. Qu, L. Gong, J. Tang, A review of conductive hydrogel used in flexible strain sensor, *Materials* 13 (2020) 3947, <https://doi.org/10.3390/ma13183947>.
- [22] K. Tao, Z. Chen, J. Yu, H. Zeng, J. Wu, Z. Wu, Q. Jia, P. Li, Y. Fu, H. Chang, W. Yuan, Ultra-sensitive, deformable, and transparent triboelectric tactile sensor based on micro-pyramid patterned ionic hydrogel for interactive human-machine interfaces, *Adv. Sci.* 9 (2022) 2104168, <https://doi.org/10.1002/advs.202104168>.
- [23] T. Liu, M. Liu, S. Dou, J. Sun, Z. Cong, C. Jiang, C. Du, X. Pu, W. Hu, Z.L. Wang, Triboelectric-nanogenerator-based soft energy-harvesting skin enabled by toughly bonded elastomer/hydrogel hybrids, *ACS Nano* 12 (2018) 2818–2826, <https://doi.org/10.1021/acsnano.8b00108>.
- [24] Y. Zeng, Y. Cheng, J. Zhu, Y. Jie, P. Ma, H. Lu, X. Cao, Z.L. Wang, Self-powered sensors driven by Maxwell's displacement current wirelessly provided by TENG, *Appl. Mater. Today* 27 (2022), 101375, <https://doi.org/10.1016/j.apmt.2022.101375>.
- [25] S. Bian, L. Hao, X. Qiu, J. Wu, H. Chang, G. Kuang, S. Zhang, X. Hu, Y. Dai, Z. Zhou, F. Huang, C. Liu, X. Zou, W. Liu, W.W. Lu, H. Pan, X. Zhao, An injectable rapid-adhesion and anti-swelling adhesive hydrogel for hemostasis and wound sealing, *Adv. Funct. Mater.* 32 (2022) 2207741, <https://doi.org/10.1002/adfm.202207741>.
- [26] C. Cai, X. Zhang, Y. Li, X. Liu, S. Wang, M. Lu, X. Yan, L. Deng, S. Liu, F. Wang, C. Fan, Self-healing hydrogel embodied with macrophage-regulation and responsive-gene-silencing properties for synergistic prevention of peritendinous adhesion, *Adv. Mater.* 34 (2022) 2106564, <https://doi.org/10.1002/adma.202106564>.
- [27] Q. Fan, Y. Nie, Q. Sun, W. Wang, L. Bai, H. Chen, L. Yang, H. Yang, D. Wei, Nanocomposite hybrid biomass hydrogels as flexible strain sensors with self-healing ability in harsh environments, *ACS Appl. Polym. Mater.* 4 (2022) 1626–1635, <https://doi.org/10.1021/acsapm.1c01433>.
- [28] T. Ke, L. Zhao, X. Fan, H. Gu, Rapid self-healing, self-adhesive, anti-freezing, moisturizing, antibacterial and multi-stimuli-responsive PVA/starch/tea polyphenol-based composite conductive organohydrogel as flexible strain sensor, *J. Mater. Sci. Technol.* 135 (2023) 199–212, <https://doi.org/10.1016/j.jmst.2022.06.032>.
- [29] K. Zhao, W. Sun, X. Zhang, J. Meng, M. Zhong, L. Qiang, M.-J. Liu, B.-N. Gu, C.-C. Chung, M. Liu, F. Yu, Y.-L. Chueh, High-performance and long-cycle life of triboelectric nanogenerator using PVC/MoS₂ composite membranes for wind energy scavenging application, *Nano Energy* 91 (2022), 106649, <https://doi.org/10.1016/j.nanoen.2021.106649>.
- [30] X. Li, X. Yin, Z. Zhao, L. Zhou, D. Liu, C. Zhang, C. Zhang, W. Zhang, S. Li, J. Wang, Z.L. Wang, Long-lifetime triboelectric nanogenerator operated in conjunction modes and low crest factor, *Adv. Energy Mater.* 10 (2020) 1903024, <https://doi.org/10.1002/aenm.201903024>.
- [31] M. Wu, X. Zheng, R. Liu, N. Hou, W.H. Afridi, R.H. Afridi, X. Guo, J. Wu, C. Wang, G. Xie, Glowing sucker octopus (*Stauroteuthis syrtensis*)-inspired soft robotic gripper for underwater self-adaptive grasping and sensing, *Adv. Sci.* 9 (2022) 2104382, <https://doi.org/10.1002/advs.202104382>.
- [32] Y.-C. Lai, J. Deng, R. Liu, Y.-C. Hsiao, S.L. Zhang, W. Peng, H.-M. Wu, X. Wang, Z. L. Wang, Actively perceiving and responsive soft robots enabled by self-powered, highly extensible, and highly sensitive triboelectric proximity- and pressure-sensing skins, *Adv. Mater.* 30 (2018) 1801114, <https://doi.org/10.1002/adma.201801114>.
- [33] H. Jia, E. Mailand, J. Zhou, Z. Huang, G. Dietler, J.M. Kolinski, X. Wang, M. S. Sakar, Universal soft robotic microgripper, *Small* 15 (2019) 1803870, <https://doi.org/10.1002/smll.201803870>.
- [34] S. Zhang, B. Zhang, D. Zhao, Q. Gao, Z.L. Wang, T. Cheng, Nondestructive dimension sorting by soft robotic grippers integrated with triboelectric sensor, *ACS Nano* 16 (2022) 3008–3016, <https://doi.org/10.1021/acsnano.1c10396>.
- [35] J. Chen, K. Han, J. Luo, L. Xu, W. Tang, Z.L. Wang, Soft robots with self-powered configurational sensing, *Nano Energy* 77 (2020), 105171, <https://doi.org/10.1016/j.nanoen.2020.105171>.
- [36] Z. Shen, Z. Zhang, N. Zhang, J. Li, P. Zhou, F. Hu, Y. Rong, B. Lu, G. Gu, High-stretchability, ultralow-hysteresis conducting polymer hydrogel strain sensors for soft machines, *Adv. Mater.* 34 (2022) 2203650, <https://doi.org/10.1002/adma.202203650>.
- [37] T. Jin, Z. Sun, L. Li, Q. Zhang, M. Zhu, Z. Zhang, G. Yuan, T. Chen, Y. Tian, X. Hou, C. Lee, Triboelectric nanogenerator sensors for soft robotics aiming at digital twin applications, *Nat. Commun.* 11 (2020) 5381, <https://doi.org/10.1038/s41467-020-19059-3>.
- [38] Y. Yao, C. Yin, S. Hong, H. Chen, Q. Shi, J. Wang, X. Lu, N. Zhou, Lanthanide-ion-coordinated supramolecular hydrogel inks for 3D printed full-color luminescence and opacity-tuning soft actuators, *Chem. Mater.* 32 (2020) 8868–8876, <https://doi.org/10.1021/acs.chemmater.0c02448>.
- [39] H.C. Yu, S.Y. Zheng, L. Fang, Z. Ying, M. Du, J. Wang, K. Ren, Z.L. Wu, Q. Zheng, Reversibly transforming a highly swollen polyelectrolyte hydrogel to an extremely tough one and its application as a tubular grasper, *Adv. Mater.* 32 (2020) 2005171, <https://doi.org/10.1002/adma.202005171>.
- [40] Y. Yang, K. Vella, D.P. Holmes, Grasping with kirigami shells, *Sci. Robot.* 6 (2021) eabd6426, <https://doi.org/10.1126/scirobotics.abd6426>.
- [41] B. Ying, R.Z. Chen, R. Zuo, J. Li, X. Liu, An anti-freezing, ambient-stable and highly stretchable ionic skin with strong surface adhesion for wearable sensing and soft robotics, *Adv. Funct. Mater.* 31 (2021) 2104665, <https://doi.org/10.1002/adfm.202104665>.
- [42] M.J. Bathaei, R. Singh, H. Mirzajani, E. Istif, M.J. Akhtar, T. Abbasiasl, L. Beker, Photolithography-based microfabrication of biodegradable flexible and stretchable sensors, *Adv. Mater.* (2022) 2207081, <https://doi.org/10.1002/adma.202207081>.
- [43] J. Wei, Y. Zhao, S. Yu, J. Du, X. Hu, G. Bai, Z. Wang, Environment-friendly dual-network hydrogel dust suppressant based on xanthan gum, polyvinyl alcohol and acrylic acid, *J. Environ. Manag.* 295 (2021), 113139, <https://doi.org/10.1016/j.jenvman.2021.113139>.
- [44] Q. Zhang, X.M. Hu, M.Y. Wu, M.M. Wang, Y.Y. Zhao, T.T. Li, Synthesis and performance characterization of poly (vinyl alcohol)-xanthan gum composite hydrogel, *React. Funct. Polym.* 136 (2019) 34–43, <https://doi.org/10.1016/j.reactfunctpolym.2019.01.002>.
- [45] J. Chen, M. Zheng, K.B. Tan, J. Lin, M. Chen, Y. Zhu, Polyvinyl alcohol/xanthan gum composite film with excellent food packaging, storage and biodegradation capability as potential environmentally-friendly alternative to commercial plastic bag, *Int. J. Biol. Macromol.* 212 (2022) 402–411, <https://doi.org/10.1016/j.ijbiomac.2022.05.119>.
- [46] I. Caldeira, A. Lüdtke, F. Tavares, C. Cholant, R. Balboni, W.H. Flores, A. Galio, A. Pawlicka, C.O. Avellaneda, Ecologically friendly xanthan gum-PVA matrix for solid polymeric electrolytes, *Ionics* 24 (2018) 413–420, <https://doi.org/10.1007/s11581-017-2223-6>.
- [47] Z.L. Wang, A.C. Wang, On the origin of contact-electrification, *Mater. Today* 30 (2019) 34–51, <https://doi.org/10.1016/j.mattod.2019.05.016>.
- [48] R. Guo, Y. Fang, Z. Wang, A. Libanori, X. Xiao, D. Wan, X. Cui, S. Sang, W. Zhang, H. Zhang, J. Chen, Deep learning assisted body area triboelectric hydrogel sensor network for infant care, *Adv. Funct. Mater.* 32 (2022) 2204803, <https://doi.org/10.1002/adfm.202204803>.
- [49] G. Chen, J. Huang, J. Gu, S. Peng, X. Xiang, K. Chen, X. Yang, L. Guan, X. Jiang, L. Hou, Highly tough supramolecular double network hydrogel electrolytes for an artificial flexible and low-temperature tolerant sensor, *J. Mater. Chem. A* 8 (2020) 6776–6784, <https://doi.org/10.1039/D0TA00002G>.